Human Molecular Genetics, 2008, Vol. 17, No. 15 **2345–2356**
doi:10.1093/hmg/ddn135
Advance Access published on May 14, 2008

Neurological deficits and glycosphingolipid accumulation in saposin B deficient mice

Ying Sun[1,4], David P. Witte[3,5], Huimin Ran[1], Matt Zamzow[1], Sonya Barnes[1], Hua Cheng[6], Xianlin Han[6], Michael T. Williams[2,4], Matthew R. Skelton[2,4], Charles V. Vorhees[2,4] and Gregory A. Grabowski[1,4,*]

[1]Division of Human Genetics, [2]Division of Neurology and [3]Division of Pediatric Pathology, Cincinnati Children's Hospital Medical Center, Cincinnati, OH, USA, [4]Department of Pediatrics and [5]Department of Pathology, University of Cincinnati College of Medicine, Cincinnati, OH 45229-3039, USA and [6]Department of Medicine, Washington University School of Medicine, St Louis, MO 63110, USA

Received March 13, 2008; Revised and Accepted April 21, 2008

Saposin B derives from the multi-functional precursor, prosaposin, and functions as an activity enhancer for several glycosphingolipid (GSL) hydrolases. Mutations in saposin B present in humans with phenotypes resembling metachromatic leukodystrophy. To gain insight into saposin B's physiological functions, a specific deficiency was created in mice by a knock-in mutation of an essential cysteine in exon 7 of the prosaposin locus. No saposin B protein was detected in the homozygotes (B−/−) mice, whereas prosaposin, and saposins A, C and D were at normal levels. B−/− mice exhibited slowly progressive neuromotor deterioration and minor head tremor by 15 months. Excess hydroxy and non-hydroxy fatty acid sulfatide levels were present in brain and kidney. Alcian blue positive (sulfatide) storage cells were found in the brain, spinal cord and kidney. Ultrastructural analyses showed lamellar inclusion material in the kidney, sciatic nerve, brain and spinal cord tissues. Lactosylceramide (LacCer) and globotriaosylceramide (TriCer) were increased in various tissues of B−/− mice supporting the *in vivo* role of saposin B in the degradation of these lipids. CD68 positive microglial cells and activated GFAP positive astrocytes showed a proinflammatory response in the brains of B−/− mice. These findings delineate the roles of saposin B for the *in vivo* degradation of several GSLs and its primary function in maintenance of CNS function. B−/− provide a useful model for understanding the contributions of this saposin to GSL metabolism and homeostasis.

INTRODUCTION

The prosaposin locus encodes in tandem four related ~80 amino acid proteins, the saposins, with activation effects on specific glycosphingolipid (GSL) hydrolases (1–4). Saposins are proteolytically cleaved from the protein precursor, prosaposin, in the late endosomes and lysosomes (5–7). The stability of each saposin is maintained by three conserved disulfide bridges (8). The genetic deficiencies of individual saposins or prosaposin highlight their physiological importance in GSL degradation (9–12). Saposin A is essential to the metabolism of β-galactosylceramide (GalCer) (13) and its deficiency leads to a late-onset form of globoid cell leukodystrophy or Krabbe disease (14). Saposin B has lipid transfer properties (15) and stimulates the degradation of sulfatide and other glycolipids (16). Saposin B deficiency in humans leads to sulfatide accumulation and a metachromatic leukodystrophy (MLD)-like disease similar to that observed with arylsulfatase A (ASA) deficiency, its cognate enzyme (17). Saposin C activates acid β-glucosidase (EC 3.2.1.45, GCase) and deficiency of saposin C leads to Gaucher-like diseases due to diminished GCase activity (10,18,19). Saposin D

*To whom correspondence should be addressed at: Division of Human Genetics, Cincinnati Children's Hospital Medical Center, 3333 Burnet Avenue, MLC 4006, Cincinnati, OH 45229-3039, USA. Tel: +1 5136367290; Fax: +1 5136362261; Email: greg.grabowski@cchmc.org

enhances acid ceramidase activity (20). In mice, saposin D deficiency is associated with ceramide accumulation, partial loss of Purkinje cells and impaired urinary system function (21). This phenotype does not mimic the embryonic lethality exhibited by mice with complete deficiency of acid ceramidase, saposin D's cognate enzyme (22). A complete deficiency of human prosaposin results in the storage of multiple GSLs and early lethality (11,12). Targeted disruption of prosaposin in the mouse causes a complex neurodegenerative phenotype resulting in a severe leukodystrophy with accumulation of GSLs in both neurons and microglial cells (23).

Saposin B facilitates partial extraction of GSLs from membranes and presents sulfatides and globotriaosylceramide (TriCer or Gb3) to ASA and α-galactosidase A, respectively, for cleavage (24–26). The dimeric shell structure of saposin B is critical for its binding to these hydrophobic lipids (26). Both saposin B and C have *in vitro* activation effects on GalCer-β-galactosidase, and GM1-β-galactosidase, as well as on the β-galactosidase for hydrolysis of lactosylceramide (LacCer) (27). Saposin B may also function as a transporter of lipid substrates to these enzymes (15). In a recent study, saposins A–D have been reported to promote lipid binding to the CD1d, a molecule important for NKT cell development (28). Saposin B is found to be most efficient at facilitating this interaction (29).

MLD is an autosomal recessive neurodegenerative lysosomal disease caused by defective ASA activity (30). The MLD variants are characterized by accumulation of sulfatides, progressive demyelination and extensive white matter damage (30). A few cases of MLD-like disease are caused by saposin B deficiency. The saposin B defects arises from various mutations in the saposin B domain of prosaposin that produce substitutions for critical cysteine residues, insertions, transversions or obliteration of a glycosylation site (31,32). Human patients with saposin B deficiency have elevated sulfatide levels in kidney and brain, and variable neurological phenotypes (31).

Deficiency of ASA enzymatic activity caused by targeted disruption of ASA in mice results in diminished *in vivo* enzyme activity, accumulation of sulfatide in white matter and a neurological phenotype that manifests by 24 months of age. There is no apparent demyelination observed in these mice (33). One specific abnormality includes total absence of auditory brain stem potentials. ASA−/− mice resemble MLD patients biochemically, however, the pathological processes are much slower and milder.

To explore the *in vivo* effects and interactions of the saposins, a series of saposin mutant mice have been created with single (14,21) or double saposin deficiencies (34). Here, mice with deficiency of saposin B were characterized for GSL metabolism and phenotypic development. This model provides insight into the essential roles of saposin B in GSL metabolism.

RESULTS

Generation and verification of saposin B targeting

Saposin B deficient mice (B−/−) were created by a knock-in of cysteine 4 to create a phenylalanine substitution in exon 7 of the prosaposin locus that corresponds to the saposin B domain (Fig. 1A). The mutation (Cys→Phe) was expected to destroy one of the three essential disulfide bonds of saposin B as had been the previous experience with other saposins (14,21,34). The recombinant ES clones were screened by PCR and confirmed by Southern blot analyses (Fig. 1B). The mutation in the ES clone was verified by PCR and DNA sequencing. The resulting F1 heterozygous mice were bred with Zp3-Cre transgenic mice to remove the floxed *neo* in the female germline (see Materials and Methods). The Zp3-Cre was subsequently outbred by crosses into wild-type (WT) C57BL/6J mice and confirmed by PCR (Fig. 1C).

RT–PCR of brain RNA verified that prosaposin mRNA was expressed at WT levels in saposin B−/− mice (Fig. 1D). Immunoblotting using antibodies specific to each saposin demonstrated the absence of saposin B protein, whereas prosaposin and saposins A and D were expressed at WT levels in B−/− mice tissues (Fig. 2). Saposin C levels in B−/− fibroblast cells were slightly higher (1.4-fold) than those in WT.

Phenotype of saposin B−/− mice

The onset of neurological impairment in B−/− mice was at ∼12 months of age as manifested by an unsteady gait. When suspended inverted by the tail, the B−/− mice reflexively grasped and tucked their hind-limbs to their body, whereas WT mice spread their hind-limbs and remained hanging downward (Fig. 3A). In addition, B−/− mice exhibited agitation and head tremor while standing (Fig. 3B). Ataxia and intermittent shivering was observed by 15 months. Adult B−/− mice had a body weight of 86% of WT littermates and survived up to 23 months. Male and female B−/− mice had normal fertility and no sex-specific differences were observed in phenotype or biochemistry.

Neurobehavioral assessment in saposin B−/− mice

The narrow bridges test evaluates balance and motor performance. To avoid possible sex variation, only male mice were used in the study. B−/− mice showed progressive increases in latency to cross the beams and also in hind-limb slips on 5 and 12 mm square beams. At 2 months, increases in slips reached statistical significance on the 12 mm square beam. A significant increase in latency was shown by 12 months that was consistent with the decline of motor function in B−/− mice at this age. By 15 months, the ability to cross the beam was greatly diminished (Fig. 3C). On the 5 mm square beam, 90% of the B−/− mice at 15 months failed to maintain their balance and fell off the beam. The tests on the 25 mm square, and the 11 and 17 mm round beams showed significant increases in slips or latency to cross in 12 and 15-month-old B−/− mice (data not shown). Locomotor activity in the same mice was tested for general exploration and adaptation. There were no significant differences in locomotor activity between B−/− and WT mice at any of the ages tested (data not shown). Long-term potentiation (LTP) was measured to assess hippocampal plasticity, and no significant differences were observed in B−/− mice in hippocampal LTP compared with WT at 15 month of age

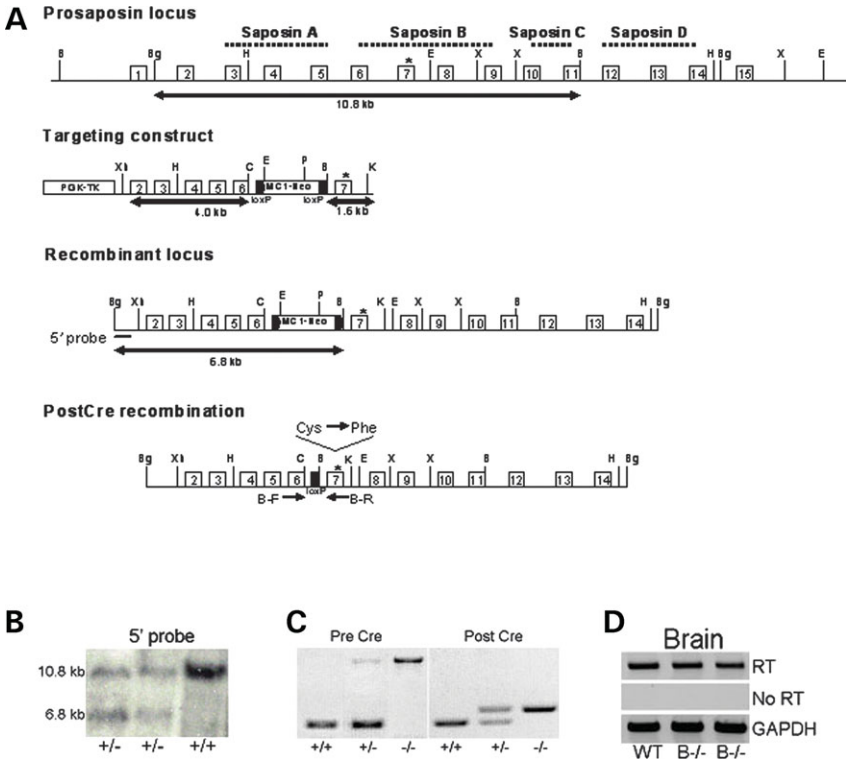

Figure 1. Saposin B knock-in targeting construct and verification. (**A**) Schematic map of saposin B targeting construct shows that the mutation in saposin B (Cys→Phe) located in exon 7. Individual saposins are encoded by the exons as indicated. The mutation destroys one of three disulfide bridges in saposin B that leads to a deficiency of the saposin B protein. The *neo* gene was removed by recombination on *lox*P sites through cross breeding of saposin B heterozygotes and Zp3-Cre transgenic mice. B, *Bam*H I; Bg, *Bgl* II; H, *Hin*d III; E, *Eco*R I; X, *Xba* I; P, *Pvu* II; C, *Cla* I; K, *Kpn* I; Xh, *Xho* I. *=mutation site. (**B**) Correct targeting of ES cells was confirmed by Southern blot using 5′ probe. The ES cell clone DNAs were digested with BamH I/Bgl II. (**C**) PCR genotyping of saposin B mice before and after Cre recombination using primers B-F and B-R across the *lox*P sites. (**D**) RT–PCR of brain RNA from WT and B−/− mice showed normal level of prosaposin RNA in B−/− mice. RT, reverse transcription. No RT, RT reaction without reverse transcriptase as a negative control. The GAPDH was an internal control.

(Fig. 4). These results demonstrated that B−/− mice had progressive decline in balance and motor coordination on the narrow bridges test, but general exploration and hippocampal LTP were similar to WT.

Histological and ultrastructural analyses

Hematoxylin and eosin (H&E) stained sections of 15-month-old B−/− mice showed inclusions in a few neurons of spinal cord, brain stem (Fig. 5) and white matter of cerebellum (data not shown). Acoustic ganglion cells in the inner ear also had storage inclusions (Fig. 5). Neuronal cells in dorsal root ganglion contained foamy inclusion material (Fig. 5). To assess the activation of macrophage/microglial cells, anti-CD68 antibody was used to stain the sections. CD68 is an intracellular membrane glycoprotein expressed in quiescent and activated tissue macrophages (35). Positive CD68 staining cells were observed in spinal cord, sciatic nerve, kidney and various regions of brain including thalamus, cortex, cerebellum and brain stem (Fig. 6). Liver, spleen and lung in B−/− mice had background levels of CD68 signal comparable to WT mice. GFAP is an astrocyte marker and enhanced GFAP signal indicates astrogliosis or activated astrocytes. Using anti-GFAP antibody, strong signals were present in the brain stem, corpus callosum, thalamus (Fig. 6), spinal cord and cerebellum (data not shown) of B−/− mice relative to age-matched WT sections. Activation of microglial cells and astrocytes demonstrates proinflammatory responses in the CNS of B−/− mice.

In 15-month-old B−/− mice, strong alcian blue staining was observed in the brain stem, cortex, cerebellum, thalamus and spinal cord, indicating the presence of acidic sulfated substances (Fig. 7A). Kidney tubules also stained positive for alcian blue (Fig. 7A). Liver, lung, pancreas, thymus and spleen were negative for alcian blue staining. Observable sulfatide accumulation began in the kidney at 7 weeks, in the spinal cord at 12 weeks and in the brain at 24 weeks (data not shown). To characterize the cell types containing sulfatide, consecutive spinal cord sections were stained with alcian blue and cell-specific markers, including: CD68, a microglial cell marker, myelin basic protein (MBP), an oligodendrocyte marker, and anti-NeuN antibody, a neuronal nuclei marker (Fig. 7B). Alcian blue staining cells were in the MBP positive region. Few CD68 stained microglia cells contained alcian blue staining materials. Neuronal soma was free of alcian blue, but such staining was detected on the neuronal processes. These results provide evidence for excess acidic sulfated substances primarily in oligodendrocytes.

Ultrastructural analyses revealed large amounts of storage material in the kidney proximal and distal tubular epithelia

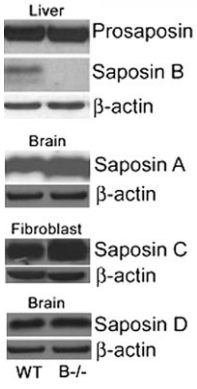

Figure 2. Saposin proteins in representative tissues of saposin B−/− mice. No saposin B was detected, whereas prosaposin was at WT levels in liver using anti-mouse saposin B antibody. Saposins A and D were at normal levels in B−/− brains detected with anti-mouse saposin A or saposin D antibodies, respectively. Using anti-mouse saposin C antibody, saposin C in B−/− fibroblast cells was slightly increased compared with WT controls.

cells (Fig. 8A–C), while mesangial cells appeared normal. The storage materials were heterogeneous aggregates of variable sized granular material and multivesicular bodies. Oligodendrocytes in brain stem, next to myelin process, were filled with heterogeneous membranous material surrounding more electron lucent material (Fig. 8D). Storage materials in oligodendrocytes and neuronal processes also were found in other regions of brain and spinal cord. Neurons in B−/− brain stem and spinal cord contained a few scattered inclusion bodies (Fig. 8E). The Schwann cells in sciatic nerve had inclusion bodies composed of large vacuoles mixed with electron dense amorphous material (Fig. 8F). Myelin layering was normal in B−/− mice (Fig. 8F). Consistent with these results, the level of MBP, a component of myelin sheath, was not altered in B−/− mice as assessed by immunoblotting (data not shown). This result suggests that sulfatide accumulation has no apparent adverse effects on myelin sheath integrity.

GSL analyses

Resolution of lipids on thin-layer chromatography (TLC) showed a slight increase of LacCer in B−/− liver relative to the elevated levels in the prosaposin knock-out (PS−/−) mice (Fig. 9A). Elevated sulfatide was detected in the kidney, lung (Fig. 9B) and brain (not shown). A moderate increase of TriCer or Gb3 was observed in the kidney (Fig. 9B). The cerebral cortex displayed levels of gangliosides (GM1, GM2, GM3, GD 1a and 1b, GT1b) comparable to WT controls (Fig. 9C). In addition, increased amounts of sulfatide were in the urine of B−/− mice (data not shown).

The composition of accumulated sulfatide was analyzed by Electrospray ionization tandem mass spectrometry (ESI/MS). Increases in non-hydroxy fatty acid (NFA) and hydroxyl fatty acid (HFA) sulfatides were detected in kidney and brain of B−/− mice. At 48 weeks, B−/− mice kidney contained 5.1- and 2.3-fold increases of C20–C24 NFA and HFA sulfatide, respectively (Fig. 10A). To reduce background levels of sulfatide in white matter, the cerebral cortex and hippocampus were dissected and analyzed for sulfatide accumulation (Fig. 10B). Most of the HFA sulfatides (C18–C24) showed marked increases. At 14.5 months of age the major accumulated NFA sulfatide species were C18 and C24 in the cortex and hippocampus. Overall, ∼2-fold increases in total HFA and NFA sulfatides were present in B−/− mouse brain samples. In the brain, C18 sulfatide was the major species affected, whereas long fatty acid acyl chain sulfatides predominated in the kidney. In contrast to the kidney, the NFA sulfatide levels in brain were higher than HFA sulfatide. Ceramide levels were unchanged in the brain and kidney of B−/− mice.

DISCUSSION

Genetic deficiencies of individual saposins (A, B, C and D) lead to lysosomal storage diseases (9,11,14,17,21). About 10 cases of saposin B deficiency states have been described in humans (31,32). To understand the *in vivo* functions of saposin B, mice were generated by introducing a point mutation into the saposin B domain of the prosaposin gene. This mutation disrupted a conserved disulfide bond that led to an unstable/undetectable saposin B protein, but preserved prosaposin, and saposin A, C and D processing and function. This strategy was also used to generate the saposin A, D and CD deficient mice (14,21,34), and facilitated the *in vivo* assessment of isolated saposin deficiency states in various organs.

The B−/− mice mimicked the biochemistry and phenotype of the human disease. Similar to human patients (31), B−/− mice developed neurological impairment including ataxia, head tremor and impaired neuromotor coordination. The early onset severe and late onset variants of saposin B deficiency have phenotypes resembling MLD with normal ASA activity (31). Furthermore, the point substitution and aberrant splicing mutations described in humans lead to a deficiency of mature saposin B with no effect on precursor transport and processing (36), but manifest excesses of Gb3 (TriCer), LacCer and GM3 in cultured fibroblasts from affected patients (31,37). Urine from these patients also contains elevated levels of sulfatide, Gb3 and digalactosylceramide (37). These findings are similar to those of the B−/− mouse. Electron microscopic findings in B−/− mice showed similar inclusion bodies as reported in humans (32). However, the disease course in mice was more slowly progressive than humans, suggesting substrate turnover differences between mice and humans as has been observed in Gaucher disease point mutation models in mice (38).

The predominant function of saposin B was in sulfatide degradation. However, the accumulation of LacCer and Gb3 (∼10–20%) in B−/− mice demonstrated that saposin B also is involved in degradation of these lipids. This finding indicates that saposin B does have *in vivo* functions in assisting α-galactosidase A and the β-galactosidase(s) involved in Gb3 and LacCer degradation, respectively, but these roles are minor in most tissues. LacCer is increased >2-fold and is the major lipid accumulated in the PS−/− mice (23), and is likely a major contributor to the pathogenesis of the prosaposin deficiency. The effects of the increases in LacCer and

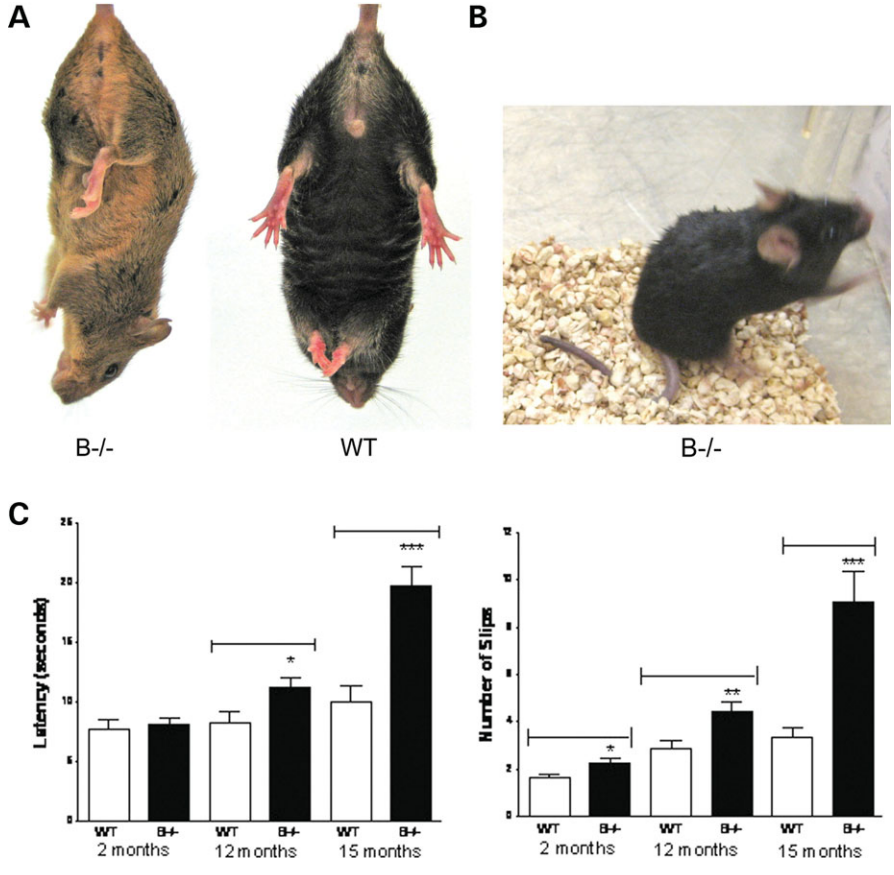

Figure 3. Phenotypes of saposin B −/− mice. (**A**) Saposin B −/− mice exhibited hind-limb clasping during tail hanging by 15 months and (**B**) head tremor was evident at 22 months. (**C**) Narrow bridges test. B−/− mice were tested on 12 mm^2 square beam. The latency (left) and foot slips (right) in B−/− became progressively different from WT with increasing age. Male mice were used in the tests. WT, $n = 17$; B−/−, $n = 26$. $^{*}P < 0.01$; $^{**}P < 0.001$; $^{***}P = 0.0001$ (Student's *t*-test).

Gb3 in the B−/− mice are unknown, but may be minor, as suggested by the increases in Gb3 in the Fabry mouse model (39,40). The lipid transport functions of saposin B could be compensated by saposin C that also is involved in the degradation of the LacCer (27). In fact, slight increases in LacCer were detected in our newly generated saposin C deficient mice (Y. Sun *et al*., unpublished data). Such mouse models demonstrate overlapping functions of saposins in GSL metabolism *in vivo*.

B−/− mice had progressive accumulation of multiple GSLs, but predominantly sulfatide, in the CNS and PNS. In the brain and spinal cord, sulfatide was detected in microglial cells, oligodendrocytes and neuronal processes. A proinflammatory response was demonstrated by the presence of activated microglial cells or astrogliosis in tissues that accumulated sulfatide. This suggests that the initiating event for proinflammation in these tissues was the presence of excess sulfatide. The oligodendrocytes were the major cell types in B−/− mice brains filled with storage materials although no apparent changes were observed in myelin sheets. Both NFA and HFA sulfatide accumulated in B−/− mice. The ratio of NFA/HFA galactosylceramide has been linked to developmental programming (41) and myelin stability (42). However, there was no effect of sulfatide accumulation on myelin integrity in B−/− mice. The normal myelin structure in B−/− mice could be due to maintenance of unchanged NFA/HFA ratios despite an increase in total sulfatide.

The neuronal inclusions were observed in both ASA deficient and B−/− mice. In particular, storage inclusions were found in their acoustic neurons. Neuronal storage of sulfatide has been reported to cause hyperexcitability and axonal degeneration in mice (43). The acoustic startle response was tested in the B−/− mice, but neither WT nor B−/− mice showed adequate responses in the C57BL/6J strain. This is due to the development of deafness in this stain of mice by the age of testing. The C57BL/6J background strain is homozygous for the age-related hearing loss mutation *Cdh23*^{ahl} that causes progressive hearing loss with onset after 10 months of age (JAX mice data base).

Saposin B participates in the degradation of sulfatide by enhancing ASA activity (37). ASA null mice have slow accumulation of sulfatide and develop CNS abnormalities (33). The B−/− mouse phenotype closely resembled this phenotype and biochemistry. Both models exhibit head tremor caused by accumulation of sulfatide in CNS and normal myelin ultrastructure. Like ASA null mice, B−/− kidney had remarkable sulfatide storage in the tubule epithelial cells that was detectable as early as 7 weeks. Lung had only a slight increase in sulfatide. Other visceral organs showed no

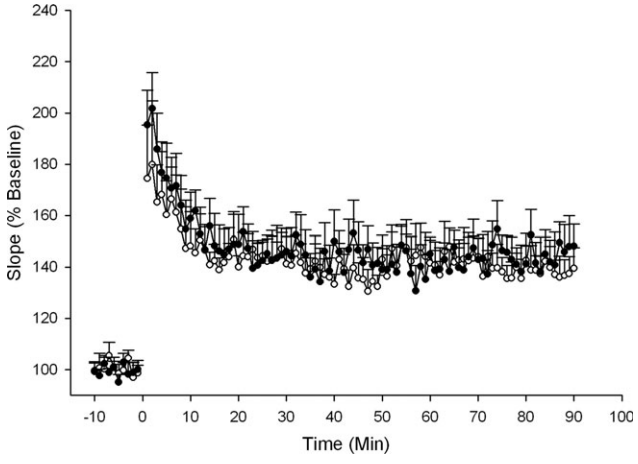

Figure 4. Long-term potentiation (LTP) analyses of saposin B−/− hippocampal regions: LTP was recorded as the slope of resulting EPSPs from the parasagittal sections (350 μm) of hippocampal CA1 region. The slopes of the EPSP (LTP) were not significantly different between 15-month-old B−/− (black circles) and WT (open circles) male mice after recording for 90 min following stimulation. WT, $n = 6$; B−/−, $n = 8$.

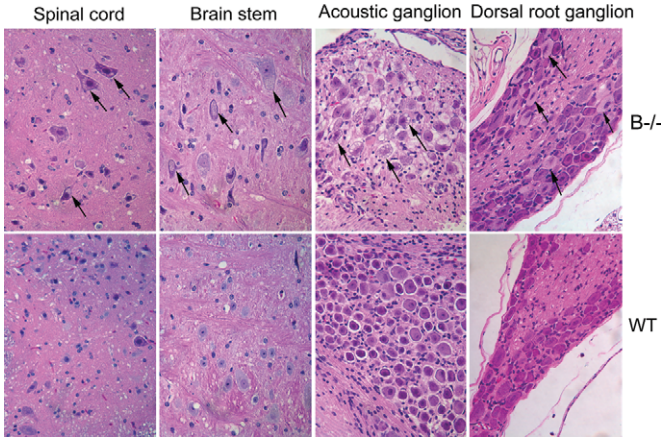

Figure 5. Storage inclusions in neural tissues from B−/− mice: H&E staining of B−/− mice neural tissue sections showed that the inclusion materials (arrows) were present in neurons of spinal cord, brain stem, acoustic ganglion of inner ear and dorsal root ganglion. WT mice did not show inclusions in matched regions. The tissues sections were from 17-month-old WT and B−/− mice.

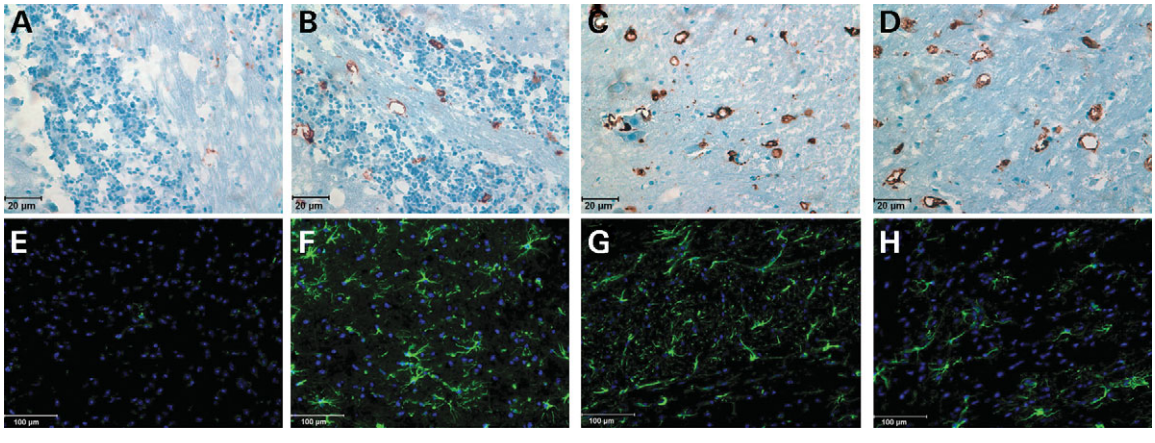

Figure 6. CD-68 and GFAP staining of CNS from B−/− mice. (Upper panel) Activated microglial cells were present in the CNS of B−/− mice. Microglial cells staining with anti-CD68 antibody (brown) in (**A**) WT and (**B**) B−/− cerebella, (**C**) B−/− spinal cord and (**D**) B−/− brain stem. The sections were counter stained with hematoxylin. (Lower panel) B−/− mice showed increased anti-GFAP (green) antibody positive cells indicating astrogliosis in several CNS regions. (**E**) WT and (**F**) B−/− thalami, (**G**) B−/− corpus colosum and (**H**) B−/− brain stem. The nuclei were stained with DAPI (blue). The tissues sections were from 17-month-old mice.

sulfatide accumulation. A unique feature of Sap B−/− mice compared with ASA deficient mice was the accumulation of LacCer and Gb3. In both mouse models, the disease is much slower developing than the human analogues. Alternative sulfatide metabolism in mice may account for these differences between humans and mice (44). Differences between mouse models and the human diseases have been observed for several lysosomal storage diseases, including acid β-glucosidase knock-out mice (45), acid β-glucosidase N370S mutant mice (38) and β-hexosaminidase A (Tay-Sach disease) mice (46).

Saposins are essential lysosomal proteins in the GSLs degradation pathway. The saposin B−/− mouse model, as well as those for other saposins (saposin A, D and CD), should provide useful tools for investigating the pathogenesis of sphingolipid storage diseases and for understanding how saposins and their cognate enzymes interact and to maintain the homeostasis of GSLs in the cell/tissues specific manner.

MATERIALS AND METHODS

Materials

The following were from commercial sources: NuPAGE 4–12% Bis–Tris gel, NuPAGE MES SDS running buffer, mouse anti-GFAP monoclonal antibody, TopoTA cloning vector (Invitrogen, Carlsband, CA); Rat anti-mouse CD68 monoclonal antibodies (Serotec, Oxford, UK); M-PER (Mammalian Protein Extraction Reagent) and BCA protein assay reagent (Pierce, Rockford, IL). Molecular Dynamics Storm 860 scanner (GE

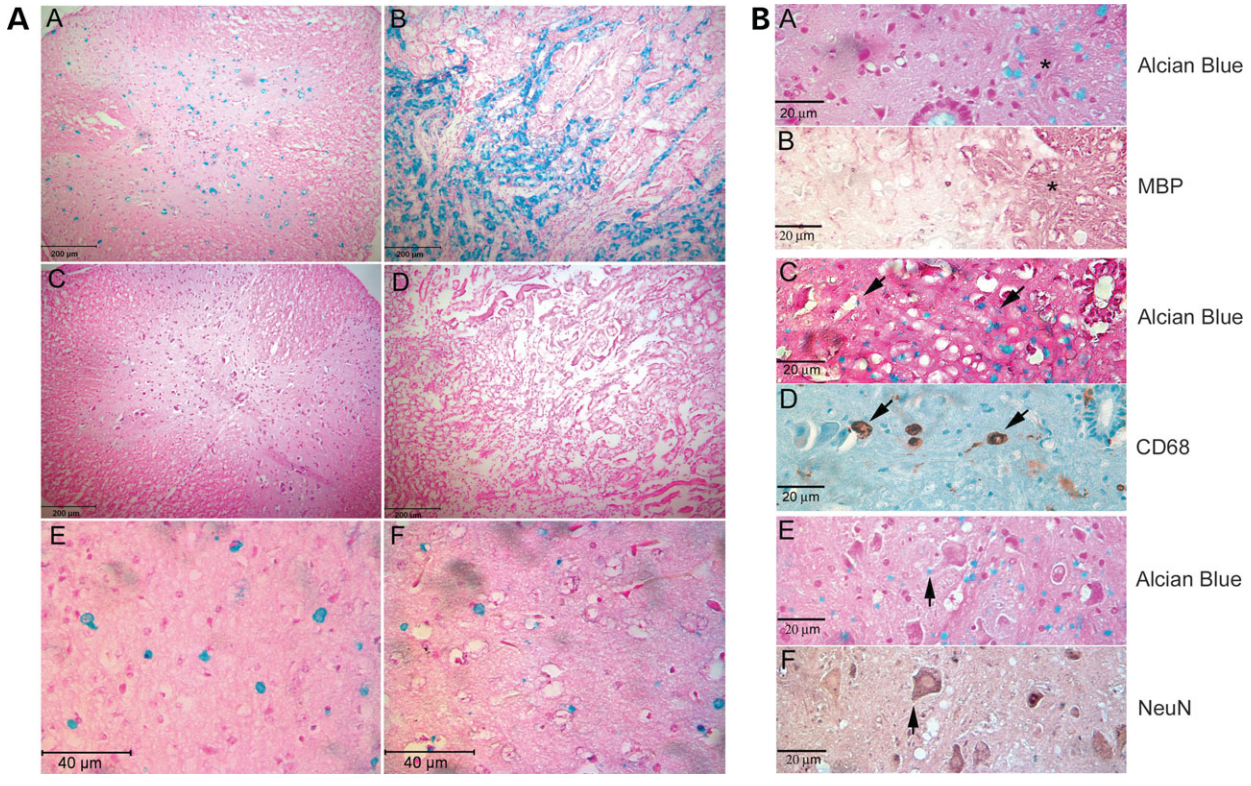

Figure 7. Alcian blue (sulfatide) staining in CNS of B−/− mice: (**A**) Alcian blue staining of B−/− tissues showed sulfatide (blue) storage in: spinal cord (A), kidney tubules (B), brain stem (E) and thalamus (F). WT spinal cord (C) and kidney (D) were free of alcian blue staining. (**B**) Consecutive spinal cord sections from B−/− mice were stained with alcian blue (A, C and E) and MBP (B), CD68 (D) and NeuN (F). (A and B) Alcian blue staining was localized to the MBP positive region (star). (C and D) CD68 positive microglial cells contained alcian blue positive material (arrows). (E and F) Alcian blue staining was on a neuronal process (arrow) and not in the neuronal soma. The tissues sections were from 15-month-old mice.

Healthcare, Chicago, IL) was used, and Hybond^{TM}-ECL^{TM} nitrocellulose membrane and ECL detection reagent (Amersham Biosciences, Piscataway, NJ). Anti-fade/DAPI, methyl green, ABC Vectastain and Alkaline phosphatase kit II (Black) were used (Vector Laboratory, Burlingame, CA). DIG Easy Hyb, Anti-digoxigenin-AP, CDP-Star, positively charged nylon membrane and Lumi-film chemiluminescent detection film were used (Roche Applied Science, Indianapolis, IN) as well as the Qiagen Quick-change II XL kit (Qiagen Inc., Valencia, CA). Restriction enzymes were from New England BioLabs (Beverly, MA). TOTALLY RNA (Ambion Inc., Austin, TX) and High capacity cDNA archive kit (Applied Biosystems, Foster City, CA) was used. FITC-conjugated goat anti-rabbit antibody and rhodamine-conjugated goat anti-rat antibody was used (ICN/CAPPEL, Aurora, OH), as was Alcian blue (Poly Scientific, Bay Shore, NY).

Construction of the targeting vector and generation of B−/− mice

The mouse prosaposin genomic DNA clones and targeting vector (OSdupdel) were kindly provided by Dr Kunihiko Suzuki. A subclone 6-1 in pBluescript vector containing exons 2-7 and subclone 4-1 with exons 4-7 was used to generate the saposin B targeting vector. Substitution of a conserved cysteine (Cys) breaks one of the three disulfide bridges in the selected saposin and results in the deficiency of that individual saposin (14,21). This strategy was adapted to produce saposin B deficiency by introducing a Cys→Phe substitution in saposin B. This was accomplished using Qiagen Quick-change II XL kit with mismatched oligonucleotide primers: B4F (5′-T GTC TCT CTG CAG TTT AAA AAC TAC GTG G-3′), B4R (5′-CCA CGT GTT TTT AAA CTG CAG ACA GAC A-3′) using the subclone 4-1 as a template. The mismatched nucleotides are underlined. The short arm *Bam*H I-*Kpn* I 1.6 kb fragment containing the saposin B mutation was generated by PCR and subcloned into the TopoTA cloning vector. The long arm *Xho* I-*Cla* I 4.0 kb fragments were generated by PCR using subclone 6-1 as a template. The product was cloned into the TA cloning vector. The saposin B targeting construct was assembled in OSdupdel containing the Polymer enhancer/herpes simplex virus thymidine kinase (MC1) promoter with the neomycin (*neo*) gene flanked by two *lox*P sites and the thymidine kinase (TK) gene driven by the 3′ phosphoglycerate kinase (*PGK*) promoter (23). The short arm (1.6 kb) containing the mutation was cloned into *Bam*H I/*Kpn* I sites downstream of MC1-*neo* in the vector, thereby forming the 3′ homologous region. The long arm (4.0 kb) released with *Eco*R I from the TA cloning vector was blunt ligated into *Nhe* I sites upstream of MC1-*neo* to form the 5′ homologous region. The sequences of long arm and short arm were validated by direct sequencing.

The targeting vector was linearized with *Not*1 and introduced into the 129/SvEv ES cell line. Recombinant ES

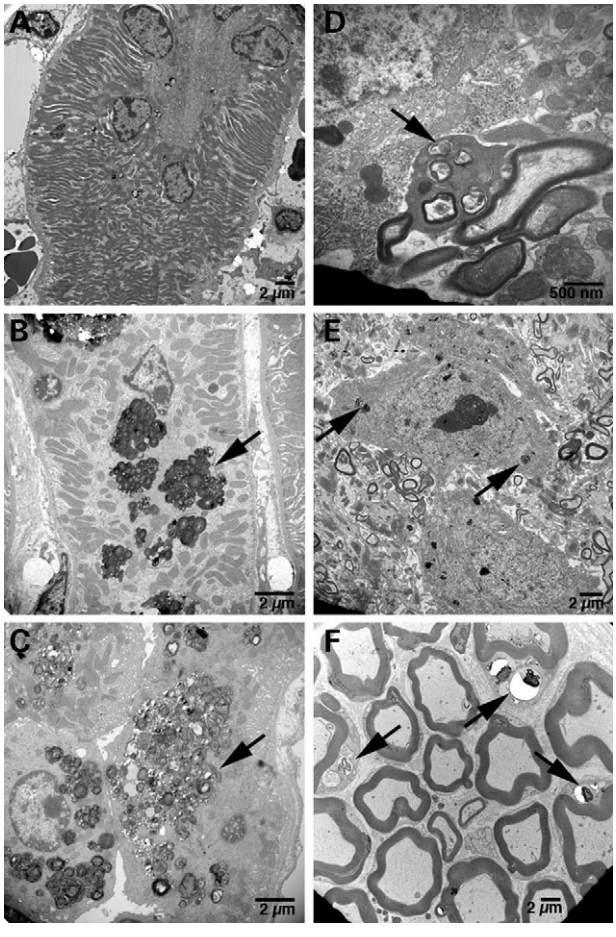

Figure 8. Ultrastructural kidney and CNS of saposin B−/− mice. (**A**) An electron micrograph of a normal proximal renal tubular cell. Rare and non specific small residual bodies were in the cytoplasm of the tubular lining cell. (**B**) Proximal renal tubular epithelial cells contained numerous large complex appearing multivesicular bodies (arrow). The storage materials consisted of aggregates of variable size heterogeneous granular material with slightly pale central cores surrounded by a rim of more electron dense amorphous material. (**C**) Renal epithelial cells from a distal tubule also contained a large amount of storage material (arrow). The material was similar to that seen in the proximal tubule in (B), although slightly less electron dense. A few of the vesicular bodies contained layers of membranous material surrounding less dense material in the central core. (**D**) An oligodendrocyte (arrow) in brain stem next to a myelinated process. The oligodendrocyte contained storage materials composed of dense membranous material surrounding more electron lucent material. (**E**) A neuron from brain stem had a few scattered inclusion bodies (arrows) representing storage materials. (**F**) A section through the sciatic nerve with myelinated fibers. The Schwann cells (arrows) contained inclusion bodies including large vacuoles mixed with electron dense amorphous material. The tissues were from 15-month-old mice.

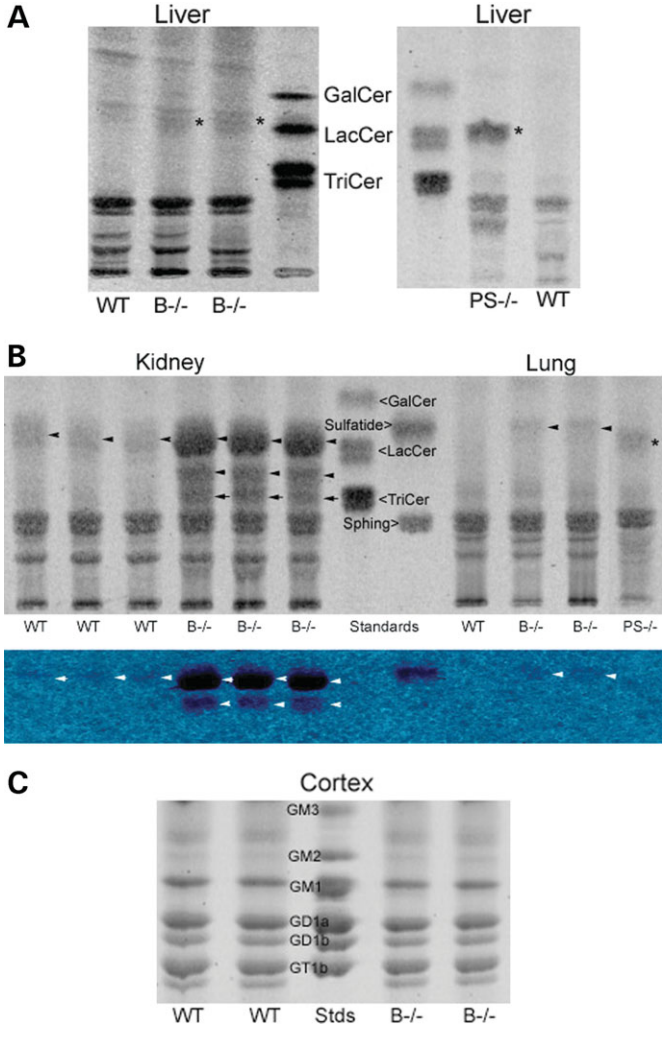

Figure 9. Glycosphingolipid analyses by TLC. (**A**) Lactosylceramide (LacCer, asterisk) was slightly increased in B−/− mice liver relative to WT, but lower than LacCer level in PS−/− mice (right panel). (**B**) Upper panel: Sulfatide (arrowheads) accumulated in B−/− kidney and was slightly elevated in B−/− lung. TriCer (arrows) was increased in B−/− kidney. Bottom panel: same plate as in the upper panel stained with Azure A to verify the sulfatide (arrowhead). (**C**) Gangliosides in B−/− mice cortex were not changed compared with WT cortex. WT and B−/− samples were from 15-month-old mice and PS−/− is from 4-week-old mice.

clones were screened by PCR analysis using the primers inside of the short arm: ABR1 (5′-GCC AGA CCT GTC AGT TTG TGA TGA A-3′) or outside of the short arm: ABR2 (5′-CTG GAG GAG TTC TAT ACG TGC CCA-3′), together with the primer in the 3′ region of *neo*, NEO3′F2 (5′-GGT GTT GGG TCG TTT GTT CGG ATC A-3′). The recombinant and WT clones generated 1.4 and 1.6 kb PCR products, respectively. The recombinant ES clones were confirmed with Southern blot analyses. The clones were digested by *Bam*H I/*Bgl* II and probed with the 5′ probe. The mutations in the recombinant clone were verified by PCR and sequencing. The correctly targeted clones were used to generate chimeric mice by microinjection into C57BL/6J blastocysts. Electroporation, ES cell culture, selection and chimera breeding were carried out by the mouse Gene-targeting service core at the University of Cincinnati. To remove the *neo* gene, the heterozygous F1 mice were cross bred to Zp3-Cre mice [C57BL/6-TgN(Zp3-Cre)93Knw; The Jackson Laboratory]. The resulting females carrying the Zp3-Cre and were saposin B deficiency heterozygotes (B+/-) were then cross bred to B+/− heterozygous males for Cre recombination between two *lox*P sites. Zp3-Cre transgene was out bred by crosses of the B+/−; ZP3-Cre with WT C57BL/6J mice. The intercross of B+/− without *neo* and without Zp3-Cre generated the saposin B−/− homozygotes. The strain of background for saposin B−/− (B−/−) was C57BL/6J/129SvEv.

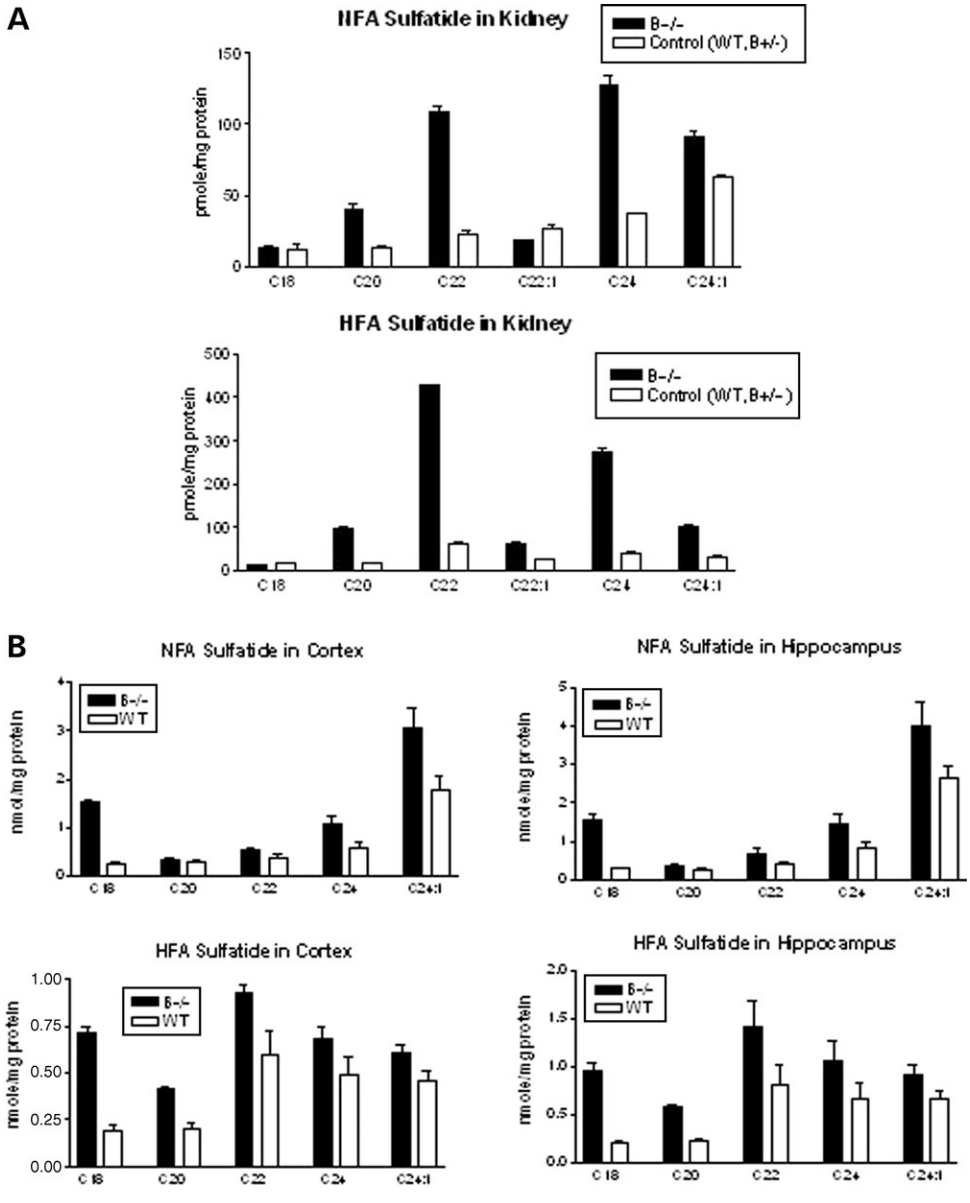

Figure 10. ESI/MS analysis of sulfatide. (**A**) Kidney. (Upper panel) Non-hydroxy (NFA) sulfatide C20, C22, C24 and C24:1 accumulated in B−/− mice compared with control samples. (Lower panel) Hydroxyl (HFA) sulfatides C20–C24:1 were increased relative to WT. Kidney samples were from 48-week-old mice. (**B**) Cortex and hippocampus. (Upper panel) NFA sulfatide C18, C24 and C24:1 were increased in B−/− mice. (Lower panel) HFA sulfatide C18-C24:1 were at higher levels than WT controls. Brain tissues were from 15-month-old mice. NFA sulfatide level was higher in cortex and hippocampus than kidney, whereas the HFA sulfatide level was greater in the kidney than brain sections. The amount of sulfatide were normalized by mg protein ($n = 3$).

Prosaposin Knock-out (PS−/−) mice (23) were used in the GSL analysis. The mice were maintained in microisolators in accordance with institutional guidelines under IACUC approval at Cincinnati Children's Research Foundation.

PCR genotyping and Southern blot analyses

PCR reactions and Southern blotting were conducted as described (34). The genotyping primers were B-F (5′-GAA GGA AGC ATT TCA CCA GGC CAC T-3′) and B-R (5′-GGA GTA ATG ACT AGT AGG GAG TGA TCA-3′). The PCR product from WT was 200 bp, and from B−/− with *neo* was 1.4 kb and without *neo* was 307 bp. Using a 5′ probe in Southern blotting, *Bgl* II/*Bam*H I digestion generated 10.8 kb WT fragment and 6.8 kb recombinant fragment.

RT–PCR

Total RNA was extracted from mouse tissues using TOTALLY RNA kit (Ambion Inc.). Reverse transcription of total RNA (10 μg) for each tissue was carried out using the High Capacity cDNA Archive Kit (Applied Biosystems) containing random hexamers primers. The reaction was for 10 min at 25°C and 120 min at 37°C. The resulting cDNA was amplified by PCR using the 10 pmol of primers PS-Left (5′-TGCAGCCTGCGAAGTGAAGC-3′) and PSm-Reverse

(5′-TTCCACACATGGCGTTTG-3′) to generate a 1.6 kb product from prosaposin cDNA. A PCR reaction using GAPDH (glyceraldehyde-3-phosphate dehydrogenase) primers was the internal control. The PCR reaction of each RNA sample without adding reverse transcriptase in RT reaction was the negative control.

Histological analyses and immunoblotting

Tissues were collected after perfused with saline, fixed in 10% formalin, embedded in paraffin, sectioned to 4 μm and stained with H&E. Karnovsky's fixative was used for ultrastructural analyses. CD68 monoclonal antibody staining was with paraformaldehyde-fixed frozen sections as described (47). For GFAP staining, paraformaldehyde-fixed tissue sections were blocked in 20% goat serum (GS), and incubated with mouse anti-GFAP monoclonal antibody (Sigma, G3893) (1/50 diluted in PBS with 20% GS). FITC-conjugated goat anti-mouse antibody (1/100 in PBS) was added to the samples. The samples were counter-stained with anti-fade/DAPI. The signals were visualized with a Zeiss Axiovert 200M with an Apotome. Alcian blue stain, which detects acidic sulfated lipids, was used to demonstrate sulfatide accumulation in tissues. Paraffin or frozen sections were rinsed in 3% acetic acid for 3 min and stained with alcian blue solution, 1% in acetic acid, pH 2.5 (Polyscientific, S111A) for 30 min. After rinsing with 3% acetic acid followed by water, sections were counterstained with Nuclear Fast Red. The paraffin sections of spinal cords were incubated with Anti-MBP (1/100; Sternberg mono Inc., SM199) and Anti-NeuN (1/100; Chemicon, MAB377), respectively. Visualization was with the ABC Vectastain kit and Alkaline phosphatase kit II according to the manufacturer(s) instructions.

GSL analyses

The GSLs in tissue samples (~100 mg wet weight) were extracted as described (47,48). Relative proportions of lipids from the tissue samples were determined by TLC with borate impregnated plates (10 cm^2 Merck HPTLC silica gel 60, 200 μm). Plates were developed in chloroform/methanol/water (65:25:4, v/v/v). The gangliosides were resolve in chloroform/methanol/0.22% $CaCl_2$ (60:35:8, v/v/v). GSLs were visualized with primulin spray (100 mg/l in 80% acetone) and blue fluorescence scanning (Storm 860, GE Healthcare). Sulfatides were detected with Azure A spray (2% in 1 mM H_2S0_4) followed by destaining with 40 mM H_2S0_4/CH_3OH (3:1, v/v) in water.

The levels of NFA and HFA sulfatide molecular species in lipid extracts of tissue samples were determined by ESI/MS using shotgun lipidomics for sphingolipid analysis (49,50). Sulfatide contents were normalized to the protein content within the same sample. Individual samples of cerebral cortex, hippocampus and kidney from three B−/− and control (WT and B+/−) mice were separately analyzed.

Behavioral studies (narrow bridges)

The mice were tested on two different shapes of wood beams during the training and test phases. Square beams (1 m) with cross sections of 25, 12 and 5 mm^2, and round beams (1 m) with diameters of 28, 17 and 11 mm were used. The horizontal beams were 50 cm above the floor. Both ends of the beam were mounted to narrow supports. The starting point of the beam was illuminated with a 125 W floodlight and two halogen lights. The end of the beam was attached to an enclosed 20 cm^2 dark box. For the training phase, the mice traversed the 12 mm^2 beam for three consecutive days, four trials per day. The first trial lasted a maximum of 2 min and each subsequent trial was a maximum of 1 min. A successful beam cross was recorded when an animal passed the second support closest to the goal box. Animals were considered to be trained when they crossed the 12 mm^2 beam in <20 s. If a mouse failed to traverse the beam on the first day, then on the second day the mouse was allowed to start trials in the middle of the beam. Once the mouse successively traversed the beam, the start position was then moved back to the original start position. The test phase began on the fourth day and each mouse in turn received two consecutive trials (up to 60 s/trial) on each square and round beam in a progression from widest to narrowest. Latency to traverse each beam and the number of times the hind feet slipped off the beam were recorded. A total of 26 B−/− male and 17 age-matched WT male mice were included in the test. The tests were started when mice were 2-month-old and repeated at 12 and 15 month.

Tail hanging reflex observations

Mice were lifted by tail to observe the legs reflex. The legs of normal mice were in 'V' position. The affected mice exhibited inward trend with legs and a clasped position.

Locomotor activity

Individual male mice (26 B−/− and 17 WT) were placed in activity chambers for 60 min. Locomotor activity was measured in a 41 × 41 × 30 cm Accuscan activity monitor equipped with 16 pairs of photodetector-LED beams along the *x* and *y* axes (Accuscan Electronics with VersaMax software, Columbus, OH). The apparatus was cleaned with 70% ethanol between animals. Horizontal activity was recorded in 5 min intervals. B−/− and WT mice were alternated between each chamber in the test to minimize time of day effects. The test was conducted under normal fluorescent light conditions. The mice were tested at 2, 12 and 15 month.

Electrophysiology

Electrophysiology was performed using the MED64 multi-electrode array system (Alpha Med Sciences, Kadoma, Japan) (51). Fifteen-month-old mice (8 B−/− male and 6 WT male) were decapitated and the brains were placed in cold artificial cerebral spinal fluid (aCSF: 124 mM NaCl, 26 mM $NaHCO_3$, 10 mM dextrose 3 mM KCl, 1.25 mM NaH_2PO_4, 2 mM $CaCl_2$ and 1 mM $MgSO_4$). Parasagittal sections (350 μm) were taken from the hippocampus and transferred to a warm (34°C) oxygenated aCSF bath for 1 h. A section was placed in the recording chamber on an 8 × 8 electrode array with the hippocampus oriented so that the CA1

region was on the array to determine LTP in the Schaffer collateral pathway. The recording chamber was perfused with warm (37°C) aCSF at a rate of 0.5 ml/min and a humidified oxygen (95%)/CO_2 (5%) mix was added to the chamber at a rate of 2 ml/min. Pair-pulse stimuli were delivered at CA1 and excitatory post-synaptic potentials (EPSPs) were recorded until stable baseline slopes were achieved for a minimum of 10 min. Following baseline recording, a theta burst stimulation (5 Hz for 2 s) was applied to the section. The slope of resulting EPSPs was recorded for 90 min following stimulation. Brain sections were recorded in duplicate for each animal and the data were averaged per animal. Data were analyzed using Performer 2.0 software (Alpha Med Sciences).

ACKNOWLEDGEMENTS

The authors thank Brian Quinn and Juying Xu for their technical assistance, Lisa McMillin, Meredith Farmer, Sabina Sylvest and Chris Woods for skilled tissue preparation and photomicrographs, and Amy Hirsch for her clerical expertise.

Conflict of Interest statement: None declared.

FUNDING

This work was supported by grants to G.A.G (R01 NS/DK 36681), M.T.W. (R01 ES 015689) and X.H. (R01 AG23168).

REFERENCES

1. Rorman, E.G., Scheinker, V. and Grabowski, G.A. (1992) Structure and evolution of the human prosaposin chromosomal gene. *Genomics*, **13**, 312–318.
2. O'Brien, J.S., Kretz, K.A., Dewji, N., Wenger, D.A., Esch, F. and Fluharty, A.L. (1988) Coding of two sphingolipid activator proteins (SAP-1 and SAP-2) by same genetic locus. *Science*, **241**, 1098–1101.
3. Collard, M.W., Sylvester, S.R., Tsuruta, J.K. and Griswold, M.D. (1988) Biosynthesis and molecular cloning of sulfated glycoprotein 1 secreted by rat Sertoli cells: sequence similarity with the 70-kilodalton precursor to sulfatide/GM1 activator. *Biochemistry*, **27**, 4557–4564.
4. Nakano, T., Sandhoff, K., Stumper, J., Christomanou, H. and Suzuki, K. (1989) Structure of full-length cDNA coding for sulfatide activator, a Co-beta-glucosidase and two other homologous proteins: two alternate forms of the sulfatide activator. *J. Biochem (Tokyo)*, **105**, 152–154.
5. Vielhaber, G., Hurwitz, R. and Sandhoff, K. (1996) Biosynthesis, processing, and targeting of sphingolipid activator protein (SAP)precursor in cultured human fibroblasts. Mannose 6-phosphate receptor-independent endocytosis of SAP precursor. *J. Biol. Chem.*, **271**, 32438–32446.
6. Leonova, T., Qi, X., Bencosme, A., Ponce, E., Sun, Y. and Grabowski, G.A. (1996) Proteolytic processing patterns of prosaposin in insect and mammalian cells. *J. Biol. Chem.*, **271**, 17312–17320.
7. Hiraiwa, M., Martin, B.M., Kishimoto, Y., Conner, G.E., Tsuji, S. and O'Brien, J.S. (1997) Lysosomal proteolysis of prosaposin, the precursor of saposins (sphingolipid activator proteins): its mechanism and inhibition by ganglioside. *Arch. Biochem. Biophys.*, **341**, 17–24.
8. Vaccaro, A.M., Salvioli, R., Barca, A., Tatti, M., Ciaffoni, F., Maras, B., Siciliano, R., Zappacosta, F., Amoresano, A. and Pucci, P. (1995) Structural analysis of saposin C and B. Complete localization of disulfide bridges. *J. Biol. Chem.*, **270**, 9953–9960.
9. Holtschmidt, H., Sandhoff, K., Kwon, H.Y., Harzer, K., Nakano, T. and Suzuki, K. (1991) Sulfatide activator protein. Alternative splicing that generates three mRNAs and a newly found mutation responsible for a clinical disease. *J. Biol. Chem.*, **266**, 7556–7560.
10. Rafi, M.A., de Gala, G., Zhang, X.L. and Wenger, D.A. (1993) Mutational analysis in a patient with a variant form of Gaucher disease caused by SAP-2 deficiency. *Somat. Cell Mol. Genet.*, **19**, 1–7.
11. Paton, B.C., Schmid, B., Kustermann-Kuhn, B., Poulos, A. and Harzer, K. (1992) Additional biochemical findings in a patient and fetal sibling with a genetic defect in the sphingolipid activator protein (SAP) precursor, prosaposin. Evidence for a deficiency in SAP-1 and for a normal lysosomal neuraminidase. *Biochem. J.*, **285**, 481–488.
12. Hulkova, H., Cervenkova, M., Ledvinova, J., Tochackova, M., Hrebicek, M., Poupetova, H., Befekadu, A., Berna, L., Paton, B.C., Harzer, K. *et al.* (2001) A novel mutation in the coding region of the prosaposin gene leads to a complete deficiency of prosaposin and saposins, and is associated with a complex sphingolipidosis dominated by lactosylceramide accumulation. *Hum. Mol. Genet.*, **10**, 927–940.
13. Harzer, K., Paton, B.C., Christomanou, H., Chatelut, M., Levade, T., Hiraiwa, M. and O'Brien, J.S. (1997) Saposins (sap) A and C activate the degradation of galactosylceramide in living cells. *FEBS Lett.*, **417**, 270–274.
14. Matsuda, J., Vanier, M.T., Saito, Y., Tohyama, J. and Suzuki, K. (2001) A mutation in the saposin A domain of the sphingolipid activator protein (prosaposin) gene results in a late-onset, chronic form of globoid cell leukodystrophy in the mouse. *Hum. Mol. Genet.*, **10**, 1191–1199.
15. Ciaffoni, F., Tatti, M., Boe, A., Salvioli, R., Fluharty, A., Sonnino, S. and Vaccaro, A.M. (2006) Saposin B binds and transfers phospholipids. *J. Lipid Res.*, **47**, 1045–1053.
16. Li, S.C., Sonnino, S., Tettamanti, G. and Li, Y.T. (1988) Characterization of a nonspecific activator protein for the enzymatic hydrolysis of glycolipids. *J. Biol. Chem.*, **263**, 6588–6591.
17. Zhang, X.L., Rafi, M.A., DeGala, G. and Wenger, D.A. (1990) Insertion in the mRNA of a metachromatic leukodystrophy patient with sphingolipid activator protein-1 deficiency. *Proc. Natl. Acad. Sci. USA*, **87**, 1426–1430.
18. Schnabel, D., Schroder, M. and Sandhoff, K. (1991) Mutation in the sphingolipid activator protein 2 in a patient with a variant of Gaucher disease. *FEBS Lett.*, **284**, 57–59.
19. Pampols, T., Pineda, M., Giros, M.L., Ferrer, I., Cusi, V., Chabas, A., Sanmarti, F.X., Vanier, M.T. and Christomanou, H. (1999) Neuronopathic juvenile glucosylceramidosis due to sap-C deficiency: clinical course, neuropathology and brain lipid composition in this Gaucher disease variant. *Acta Neuropathol. (Berl)*, **97**, 91–97.
20. Azuma, N., O'Brien, J.S., Moser, H.W. and Kishimoto, Y. (1994) Stimulation of acid ceramidase activity by saposin D. *Arch. Biochem. Biophys.*, **311**, 354–357.
21. Matsuda, J., Kido, M., Tadano-Aritomi, K., Ishizuka, I., Tominaga, K., Toida, K., Takeda, E., Suzuki, K. and Kuroda, Y. (2004) Mutation in saposin D domain of sphingolipid activator protein gene causes urinary system defects and cerebellar Purkinje cell degeneration with accumulation of hydroxy fatty acid-containing ceramide in mouse. *Hum. Mol. Genet.*, **13**, 2709–2723.
22. Li, C.M., Park, J.H., Simonaro, C.M., He, X., Gordon, R.E., Friedman, A.H., Ehleiter, D., Paris, F., Manova, K., Hepbildikler, S. *et al.* (2002) Insertional mutagenesis of the mouse acid ceramidase gene leads to early embryonic lethality in homozygotes and progressive lipid storage disease in heterozygotes. *Genomics*, **79**, 218–224.
23. Fujita, N., Suzuki, K., Vanier, M.T., Popko, B., Maeda, N., Klein, A., Henseler, M., Sandhoff, K. and Nakayasu, H. (1996) Targeted disruption of the mouse sphingolipid activator protein gene: a complex phenotype, including severe leukodystrophy and wide-spread storage of multiple sphingolipids. *Hum. Mol. Genet.*, **5**, 711–725.
24. Furst, W. and Sandhoff, K. (1992) Activator proteins and topology of lysosomal sphingolipid catabolism. *Biochim. Biophys. Acta*, **1126**, 1–16.
25. Sandhoff, K., van Echten, G., Schroder, M., Schnabel, D. and Suzuki, K. (1992) Metabolism of glycolipids: the role of glycolipid-binding proteins in the function and pathobiochemistry of lysosomes. *Biochem. Soc. Trans.*, **20**, 695–699.
26. Ahn, V.E., Faull, K.F., Whitelegge, J.P., Fluharty, A.L. and Prive, G.G. (2003) Crystal structure of saposin B reveals a dimeric shell for lipid binding. *Proc. Natl. Acad Sci. USA*, **100**, 38–43.
27. Zschoche, A., Furst, W., Schwarzmann, G. and Sanhoff, K. (1994) Hydrolysis of lactosylceramide by human galactosylceramidase and GM1-beta-galactosidase in a detergent-free system and its stimulation by sphingolipid activator proteins, sap-B and sap-C. Activator proteins stimulate lactosylceramide hydrolysis. *Eur. J. Biochem.*, **222**, 83–90.
28. Zhou, D., Cantu, C., III, Sagiv, Y., Schrantz, N., Kulkarni, A.B., Qi, X., Mahuran, D.J., Morales, C.R., Grabowski, G.A., Benlagha, K. *et al.*

(2004) Editing of CD1d-bound lipid antigens by endosomal lipid transfer proteins. *Science*, **303**, 523–527.
29. Yuan, W., Qi, X., Tsang, P., Kang, S.J., Illarionov, P.A., Besra, G.S., Gumperz, J. and Cresswell, P. (2007) Saposin B is the dominant saposin that facilitates lipid binding to human CD1d molecules. *Proc. Natl. Acad. Sci. USA*, **104**, 5551–5556.
30. Von Figura, K., Gieselmann, V. and Jaeken, J. (2001) Metachromatic Leukodystrophy. Scriver, C.R., Beaudet, A.L., Sly, W.S. and Valle, D. (Eds), *The Metabolic and Molecular Basis of Inherited Disease.*, 8th edn. McGraw-Hill, New York, **Vol. III**, pp. 3695–3724.
31. Sandhoff, K., Kolter, T. and Harzer, K. (2001) Sphingolipid Activator Proteins. Scriver, C.R., Beaudet, A.L., Sly, W.S. and Valle, D. (Eds), *The Metabolic and Molecular Basis of Inherited Disease.*, 8th edn. McGraw-Hill, New York, **Vol. III**, pp. 3371–3388.
32. Deconinck, N., Messaaoui, A., Ziereisen, F., Kadhim, H., Sznajer, Y., Pelc, K., Cecile Nassogne, M., Vanier, M.T. and Dan, B. (2007) Metachromatic leukodystrophy without arylsulfatase A deficiency: A new case of saposin-B deficiency. *Eur. J. Paediatr. Neurol*.
33. Hess, B., Saftig, P., Hartmann, D., Coenen, R., Lullmann-Rauch, R., Goebel, H.H., Evers, M., von Figura, K., D'Hooge, R., Nagels, G. *et al.* (1996) Phenotype of arylsulfatase A-deficient mice: relationship to human metachromatic leukodystrophy. *Proc. Natl. Acad. Sci. USA*, **93**, 14821–14826.
34. Sun, Y., Witte, D.P., Zamzow, M., Ran, H., Quinn, B., Matsuda, J. and Grabowski, G.A. (2007) Combined saposin C and D deficiencies in mice lead to a neuronopathic phenotype, glucosylceramide and alpha-hydroxy ceramide accumulation, and altered prosaposin trafficking. *Hum. Mol. Genet.*, **16**, 957–971.
35. Gordon, S., Lawson, L., Rabinowitz, S., Crocker, P.R., Morris, L. and Perry, V.H. (1992) Antigen markers of macrophage differentiation in murine tissues. *Curr. Top Microbiol. Immunol.*, **181**, 1–37.
36. Wrobe, D., Henseler, M., Huettler, S., Pascual Pascual, S.I., Chabas, A. and Sandhoff, K. (2000) A non-glycosylated and functionally deficient mutant (N215H) of the sphingolipid activator protein B (SAP-B) in a novel case of metachromatic leukodystrophy (MLD). *J. Inherit. Metab. Dis.*, **23**, 63–76.
37. Li, S.C., Kihara, H., Serizawa, S., Li, Y.T., Fluharty, A.L., Mayes, J.S. and Shapiro, L.J. (1985) Activator protein required for the enzymatic hydrolysis of cerebroside sulfate. Deficiency in urine of patients affected with cerebroside sulfatase activator deficiency and identity with activators for the enzymatic hydrolysis of GM1 ganglioside and globotriaosylceramide. *J. Biol. Chem.*, **260**, 1867–1871.
38. Xu, Y.H., Quinn, B., Witte, D. and Grabowski, G.A. (2003) Viable mouse models of acid beta-glucosidase deficiency: the defect in Gaucher disease. *Am. J. Pathol.*, **163**, 2093–2101.
39. Ioannou, Y.A., Zeidner, K.M., Gordon, R.E. and Desnick, R.J. (2001) Fabry disease: preclinical studies demonstrate the effectiveness of alpha-galactosidase A replacement in enzyme-deficient mice. *Am. J. Hum. Genet.*, **68**, 14–25.
40. Ohshima, T., Murray, G.J., Swaim, W.D., Longenecker, G., Quirk, J.M., Cardarelli, C.O., Sugimoto, Y., Pastan, I., Gottesman, M.M., Brady, R.O. *et al.* (1997) alpha-Galactosidase A deficient mice: a model of Fabry disease. *Proc. Natl. Acad. Sci. USA*, **94**, 2540–2544.
41. De Haas, C.G. and Lopes-Cardozo, M. (1995) Hydroxy- and non-hydroxy-galactolipids in developing rat CNS. *Int. J. Dev. Neurosci.*, **13**, 447–454.
42. Fewou, S.N., Bussow, H., Schaeren-Wiemers, N., Vanier, M.T., Macklin, W.B., Gieselmann, V. and Eckhardt, M. (2005) Reversal of non-hydroxy:alpha-hydroxy galactosylceramide ratio and unstable myelin in transgenic mice overexpressing UDP-galactose:ceramide galactosyltransferase. *J. Neurochem.*, **94**, 469–481.
43. Eckhardt, M., Hedayati, K.K., Pitsch, J., Lullmann-Rauch, R., Beck, H., Fewou, S.N. and Gieselmann, V. (2007) Sulfatide storage in neurons causes hyperexcitability and axonal degeneration in a mouse model of metachromatic leukodystrophy. *J. Neurosci.*, **27**, 9009–9021.
44. Tempesta, M.C., Salvayre, R. and Levade, T. (1994) Functional compartments of sulphatide metabolism in cultured living cells: evidence for the involvement of a novel sulphatide-degrading pathway. *Biochem. J.*, **297**, 479–489.
45. Tybulewicz, V.L., Tremblay, M.L., LaMarca, M.E., Willemsen, R., Stubblefield, B.K., Winfield, S., Zablocka, B., Sidransky, E., Martin, B.M., Huang, S.P. *et al.* (1992) Animal model of Gaucher's disease from targeted disruption of the mouse glucocerebrosidase gene. *Nature*, **357**, 407–410.
46. Phaneuf, D., Wakamatsu, N., Huang, J.Q., Borowski, A., Peterson, A.C., Fortunato, S.R., Ritter, G., Igdoura, S.A., Morales, C.R., Benoit, G. *et al.* (1996) Dramatically different phenotypes in mouse models of human Tay-Sachs and Sandhoff diseases. *Hum. Mol. Genet.*, **5**, 1–14.
47. Sun, Y., Quinn, B., Witte, D.P. and Grabowski, G.A. (2005) Gaucher disease mouse models: point mutations at the acid {beta}-glucosidase locus combined with low-level prosaposin expression lead to disease variants. *J. Lipid Res.*, **46**, 2102–2113.
48. Sun, Y., Qi, X., Witte, D.P., Ponce, E., Kondoh, K., Quinn, B. and Grabowski, G.A. (2002) Prosaposin: threshold rescue and analysis of the 'neuritogenic' region in transgenic mice. *Mol. Genet. Metab.*, **76**, 271–286.
49. Han, X. and Gross, R.W. (2005) Shotgun lipidomics: multidimensional MS analysis of cellular lipidomes. *Expert Rev. Proteomics*, **2**, 253–264.
50. Jiang, X., Cheng, H., Yang, K., Gross, R.W. and Han, X. (2007) Alkaline methanolysis of lipid extracts extends shotgun lipidomics analyses to the low-abundance regime of cellular sphingolipids. *Anal. Biochem.*, **371**, 135–145.
51. Shimono, K., Baudry, M., Ho, L., Taketani, M. and Lynch, G. (2002) Long-term recording of LTP in cultured hippocampal slices. *Neural. Plast.*, **9**, 249–254.